A Study on the Sub-Structure and Mechanical Properties of Friction Stir Processed AA 6061-T6 Joints with Ultra-Fine Grained Structure

A. Salemi Golezani[a,*], M. Esmaily[b], N. Mortazavi[c]

[a] *Department of Materials Engineering, Karaj Branch, Islamic Azad University, Alborz, Iran.*
[b] *Department of Chemical and Biological Engineering, Chalmers University of Technology, Göteborg, Sweden.*
[c] *Department of Applied Physics, Chalmers University of Technology, Göteborg, Sweden.*

ARTICLE INFO

Article history:

Received 17 Nov. 2013
Accepted 11 Jan. 2014
Available online 25 Feb. 2014

Keywords:

Friction stir processing
Aluminum alloy
Sub-structural analysis
Dislocation density

ABSTRACT

Ultra-fine grained (UFG) structure (~0.6 μm) was produced in the stir zone (SZ) of 6061-T6 aluminum alloy joints using friction stir processing (FSP) cooled by liquid nitrogen (N_2). A new experimental set-up was used to simultaneously quench the lower and upper surfaces of the samples during the processing. In addition, FSPed joints were produced using a steel backing plate at room temperature as a reference. Sub-structural studies were carried out to investigate the occurrence of dynamic recrystallization and grain growth in the weld area of the samples. The results indicate that the microstructure was not fully recrystallized as a high dislocation density (3.5×10^{14} m^{-2}) was measured in the stir zone (SZ) of rapidly cooled joints compared with that of the air-cooled joints (1.5×10^{14} m^{-2}). Moreover, rapid cooling generated a very high dislocation density of about 6.5×10^{14} m^{-2} in the thermo-mechanical affected zone (TMAZ). Accordingly, better mechanical properties were obtained in the SZ. In contrast, lower strain hardening capacity and hardening exponent values were obtained in the rapidly cooled joints where the highest fraction of low angle grain boundaries (LAGBs) and largest number of dislocations were measured.

1. Introduction

Grain refinement has been established as an effective approach to enhance the mechanical properties of metallic materials and has been the subject of numerous studies for decades. Ultra-fine grained (UFG) metals show higher yield strength, better wear resistance and exceptionally high super-plasticity compared with their coarse-grained counterparts [1-5]. They are fabricated by various methods such as mechanical alloying, severe plastic deformation (SPD) and crystallization of amorphous precursors. There have been extensive research and developments on the SPD processes of aluminum alloys, such as accumulative roll bonding (ARB), equal channel angular pressing (ECAP), high-pressure torsion (HPT), twist extrusion (TE), accumulative back extrusion (ABE), and friction stir processing (FSP) [6-9]. FSP technique, which is a local thermo-mechanical metal working process, has a great potential to refine the microstructure of

Corresponding author:
E-mail address: salemiali@kiau.ac.ir (Ali Salemi Golezani).

Table 1. The FSP parameters including transverse and rotational speeds and cooling conditions and the calculated heat inputs for each joint

Code	Processing parameters				
	Cooling	Welding speed (mm/min)	Rotational speed (rpm)	Tilt angle of the tool (degree)	Heat input (KJ/cm)
A1	Air/Steel (RT FSP)	200	1100	2.5	6.4
A2	Air/Steel (RT FSP)	200	1000	2.5	6.1
A3	Air/Steel (RT FSP)	280	1000	2.5	4.9
N1	Liquid N_2/Copper (RC FSP)	200	1500	1.5	7.1
N2	Liquid N_2/Copper (RC FSP)	100	1500	1.5	9.5

aluminum alloys [10-14]. In addition to their potential of microstructure refinement in bulk form, many efforts have been made to join aluminum alloys sheets by FSP. Inserting some elements into a groove in the samples to produce metal matrix composites (MMCs), cooling the samples using a backing plate or coolant during the process are some of the methods that can be applied to modify the microstructure of the processed regions [15-18]. There are some certain advantages in cooled FSPed joints over non-cooled ones. Examples of the advantages are: (i) the decrease in the length of heat affected zone (HAZ), (ii) as a result of grain refinement, enhanced mechanical properties such as strength and hardness of the joints to reach the values comparable with those of the base metal (BM) according to the conventional Hall-Petch relation [16].

In FSP and in the case of rapid cooling during the process, high densities of dislocations are introduced into the microstructure of the processed areas with respect to in-air welds. Similar to FSW, depending on the rate of plasticization and the cooling rate, the processed regions can be subjected to a number of metallurgical phenomena such as dynamic recovery, recrystallization and grain growth. However, the highly deformed microstructure may not undergo a complete dynamic recrystallization due to insufficient heat input. In case of incomplete recrystallization, dislocations that are present in the processed area are influential on the evolved microstructure by producing lattice distortion and strain in the grains of different processed regions. As a result, these dislocations can affect the mechanical properties of the joints. Thus, there have been attempts to study the process-induced dislocations using high resolution electron microscopes [10-12].

The 6xxx series aluminum alloys are one of the leading non-ferrous metallic materials in use and considered as one of the main option for metallic structures in various applications. Thus, their FSW/FSPed joints have been the subject of numerous investigations [19-24]. In a preliminary study [19], the authors have performed FSP on AA 7075-T6 to fabricate UFG material in bulk form. It was shown that the dislocation accumulation mainly takes place in the thermo-mechanical heat affected zone (TMAZ). Woo et al. [20] have investigated the effect of tool pin and shoulder on the microstructural softening during FSP of AA 6061-T6. They have reported that heating from the shoulder of the tool caused softening and the natural aging behavior of their investigated alloy. Rayes et al. and Elangovan et al. [21, 22] have studied the effect of multi-pass FSP on the microstructure and mechanical properties of AA 6082. They reported that by increasing the number of passes, the average misorientation angle of the grains increased which resulted in smaller recrystallized grains in the processed regions of the AA 6061-T6 joints. Woo et al. [23, 24] have quantified the dislocation density and hardening behavior of FSWed samples during and after the processing. In this regard, further investigations could be performed on the density of dislocations of UFG AA 6061-T6 FSPed joints when the material is subjected to a strong coolant media during the process. The effect of processing parameters and cooling rate on the evolved microstructure of FSPed AA 6061-T6 joints are studied. The main focus was to quantitatively evaluate the dynamic recovery, recrystallization and grain growth and their effects on the

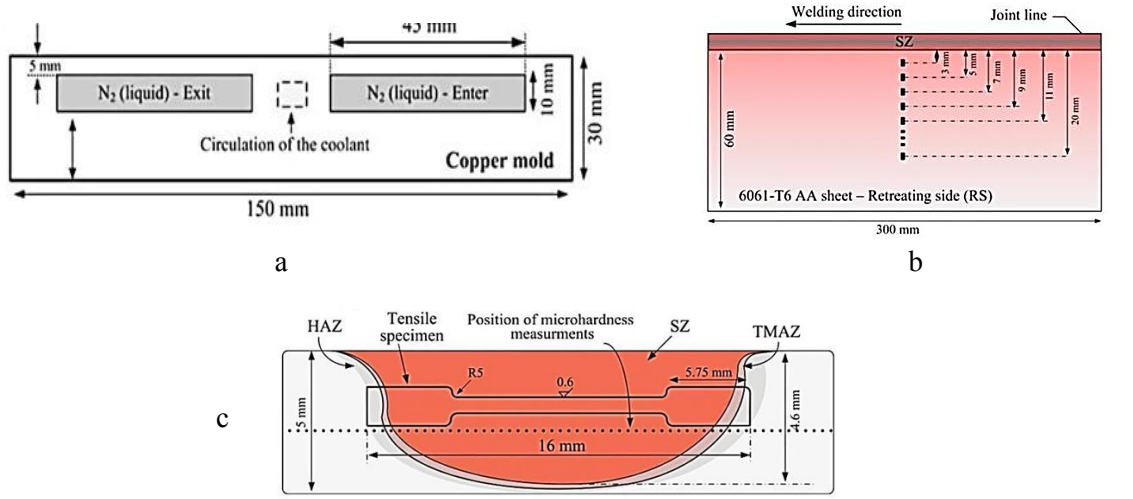

Fig. 1. (a) Copper anvil designed as backing plate used for FSP, (b) location of thermocouples with respect to the welding direction and SZ, (c) Schematic illustration of the FSW/FSP cross section, showing the location of the tensile specimens in the SZ and the possible in the central are of the microhardness measurements in the transverse section.

mechanical properties of cooled FSPed joints.

2. Experimental

A commercial AA 6061-T6 with chemical composition (wt.%) of Al-0.92Mg-0.5Si-0.33Fe-0.47Cu-0.16Cr-0.12Ti was machined to sheets with a dimension of 300×60×5 mm^3. Two types of FSPed joints were produced by beading the samples on a steel anvil with no circulating cooler agents and at room temperature (termed RT FSP in this study) and beading the samples on a copper anvil and in the presence of liquid N_2 (termed CT in this study), as shown in Table 1.

In the case of the RC FSPed joints, a new quenching methodology was designed and used. Thus, in addition to spraying the liquid N_2 on the upper surface of the samples and behind the tool, a copper anvil with three connected tunnels was produced according to the study by Cheng et al. [25]. The liquid N_2 was entering from one side and discharging from the other side of the anvil, as shown in Fig 1 (a). Therefore, the generated heat was continuously and simultaneously transferred to air from the upper side and the backing plate from the lower side of the samples as quickly as possible. It may be noted that the rotational speeds for the RC FSP joints are higher than that of the RT FSP joints.

The following parameters were the same for all the process conditions: 6.5 mm pin-tool diameter, 4.6 mm pin tool height, 0.2 mm penetration ligament, 0.2 mm plunge depth of the shoulder and 16 mm shoulder diameter. The investigated parameters and cooling conditions are given in Table 1. In-situ thermal analysis was done by nine thermocouples (k-type), as shown in Fig 1 (b). Accordingly, the cooling rates were calculated based on a method proposed by Poorhaydari et al. [26]. Visual and radiography tests (VT and RT) were carried out by utilizing NDT spec. software. After identifying sound joints, the samples were cross sectioned perpendicular to the welding direction for further microstructural and mechanical examinations.

The flawless joints were systematically examined through automated electron backscattered diffraction (EBSD) system equipped with TSL-OIM TM software, attached to the FEI SIRI-ON field emission gun JEOL 6500F scanning electron microscope. The step size in the weld area of the cooled FSPed joint was 0.04 µm. For mapping the BM and non-cooled samples a step size of 0.2 µm was selected over an area of 1.1 mm × 1.1 mm. Small grains with very few pixels were eliminated from the maps via the TSL software. A disorientation of 15° was considered to separate low-angle grain boundaries (LAGBs)

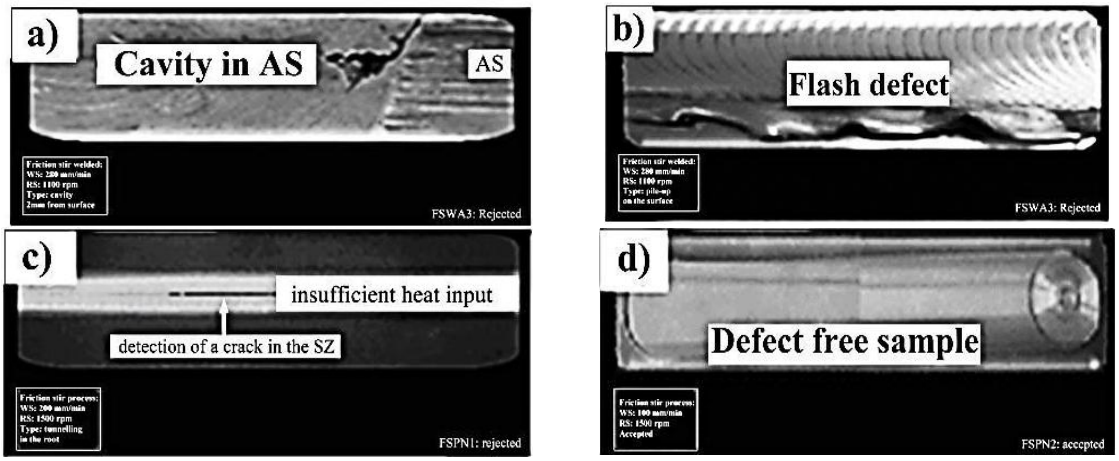

Fig. 2. Examples of some representative visual and radiography inspections of the FSWed samples. (a, b) A3: rejected due to formation of a cavity in the AS and flash defect, (c) N1: showing a crack in the root of the SZ of the joint, (d) N2: accepted joint with no macro- and micro-defects

from high-angle grain boundaries (HAGBs).

The sub-structural evolutions in different weld regions of the FSPed joints were also investigated by means of X-ray diffraction line profile analysis. Although the dislocations densities and some other sub-structural analysis can also be measured from conventional method using transmission electron microscopy (TEM) micrographs, this method of quantitative measurements suffers from some disadvantages. For instance, it is time consuming and the required statistics are not adequate. Alternatively, high-resolution microbeam X-ray diffractometer was used with a rotating anode (*Cu* $K_{\alpha}1$) radiation. The evaluation of the broadening in the x-ray diffraction peaks was done by two well-known methods, namely modified Williamson-Hall and modified Rietveld to measure the density and the character of dislocations in the processed samples in a statistical manner. Microstructural factors such as average and effective domain sizes and also micro-strain values were used to obtain quantitative data on the dislocation density of the different zones of the samples. The X-ray diffraction peak profiles were investigated by the convolutional multiple whole profile (CMWP) full pattern fitting procedure. To achieve the contribution from only physical origins to the broadening diffraction peaks, the line profiles were modified for instrumental broadening. The detailed descriptions of the methods applied in this study are comprehensively provided in the literature [27-32].

Microhardness measurements were carried out across the welds and perpendicular to the welding direction using a Buehler microhardness tester with a load of 100 gf and dwell time of 10 s. The tensile tests were done by a constant strain rate of 8×10^{-4} s^{-1} using computer-controlled Instron machine model 3385H at ambient temperature. Each reported datum of the hardness and tensile experiments is the average of four test results. The position of the microhardness measurements and tensile specimens are illustrated in Fig 1 (c).

3. Results and Discussion

In the case of RT FSPed samples, processed according to parameters presented in Table. 1, A1 and A2 welds showed no macro- and micro-scale defects. However, the A3 joint was rejected as a macro cavity or groove-like defect was observed in the stir zone (SZ) of the joint due to very low heat input. The calculated heat inputs are listed in Table 1. Also, the weld metal was piled-up (also called as flash defect) due to the fast travelling speed (Fig 2 (a, b)). In the case of RC FSPed samples, the acceptance criteria were successfully met just in the joints processed by N2 parameters (Fig 2 (c, d)).

According to the proposed heat input models [33-35] for FSW, transverse speed, rotational speed as well as shoulder diameter are the most effective parameters to determine the introduced heat input into the processed zones. It is observed that significantly higher heat inputs were needed for producing sound joints by RC FSP than those of the RT FSP as much

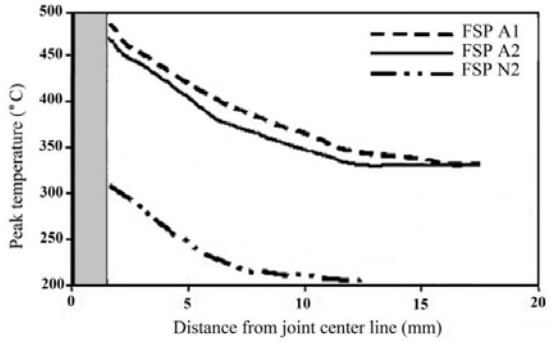

Fig. 3. Thermal profile of the FSPed joints, related to the RS

faster cooling rates were present in RC FSP. Thus, the rotational speed and tilt angle for the both N1 and N2 and travel speed just in the case of N2 was different from those of the RT FSPed joints to achieve higher heat inputs. The higher travel speed of N1 joint led to the lower heat input than that of N2 joint, indicating the great influence of the travel speed on the heat input. This caused lack of an appropriate stirring and the vertical flow of the plasticized metal in the SZ and consequently, N1 joint was rejected due to the formation of tunnel-like crack in the lower part of the SZ, i.e. the root. Further microstructural and mechanical evaluations in this study were performed on the selective or sound joints, i.e. A1, A2 and N2.

Fig 3 shows the thermal profiles of the selective FSPed samples from SZ to retreating side (RS) of the joints. The highest transient temperature, i.e. 483˚C, was related to A1 joint. The corresponding values for N1 and N2 joints are substantially lower than that of A1, which is a result of the fast cooling rate. Hence, the least softening of the cold-worked metal has taken place in the joints produced by N1 and N2 parameters. The higher rotational speed of the tool for A1 than that of A2 resulted in a slightly higher heat input per unit length (as shown in Table 1)that is in accordance with the differences in their peak temperatures. It should be noted that the measured maximum temperatures of A1 and A2 joints are high enough to entail a solution heat treatment in the alloy. The N2 joint, with the fastest cooling rate (about 65 Cs^{-1}), experienced the shortest time in its peak temperature compared with that of A1 and A2 weldments, with cooling rates of 21.5 and 23 Cs^{-1}, respectively. It is worth mentioning that faster cooling rates can be obtained by either lowering or sinking the introduced heat input into samples during the FSP. In this study, although the theoretical heat input in the FSPed joints was higher, considerably faster cooling rates were achieved by the great sinking effect obtained by the copper anvil and quenching the joints using liquid N_2.

From the visual and radiography examinations of the joints, a rotational speed of 1500 rpm and a transverse speed of 100 mm/min with a tilt angle of 1.5º are the optimum parameters to produce flawless joints when liquid N_2 is present during the processing. It should be mentioned that a wide range of processing parameters including travel speeds between 200 to 450 mm/min, rotational speeds between 1200 to 1600 rpm and tilt angles between 0 to 3º were examined in the case of RC FSP joints. However, the inspection tests revealed that a very narrow window of the FSP parameters (presented as N2 code in Table 1) can result in a high quality or flawless UFG FSPed joints by such processing condition.

Generally, from the SZ to the BM of the FSWed aluminum alloy joints, the shape of the grains are transferred from equiaxed to elongated and the size of the grains increases from a few micrometers to several tens of micrometer [36-38]. Typical microstructures of the different zones in FSWed Al-Mg-Si alloys are well-studied in the previous works [39-42]. In this study, as it was expected, the grains in the SZ of the FSWed samples were transferred to a fine recrystallized homogeneous grain structure (Fig. 4 (a)-(c)). This can be explained based on a high strain induced by severe plastic deformation and the occurrence of dynamic recovery and recrystallization processes of the deformed grains.

Fig 5 shows the grain size distribution profiles of the SZs obtained from EBSD data. As can be seen, both uniform and non-uniform microstructures with different size distribution of the grains were produced by FSP. The grain size distribution in the SZ of A1 joint covers a wide range, from 2.5 to 18 μm with an average grain size of 9 μm. The other RT FSPed joint, i.e. A2, that experienced less heat input and faster cooling rate, showed more uniform grain structure as the size of the grains are tabulated

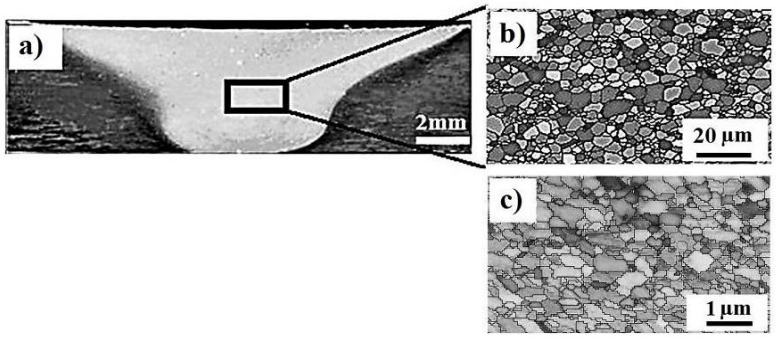

Fig. 4. (a) An overview of the cross section of a typical flawless FSPed joint, (b) EBSD map of the SZ of the A1 sample showing the HAGBs, (c) EBSD map of the SZ of the N2 sample

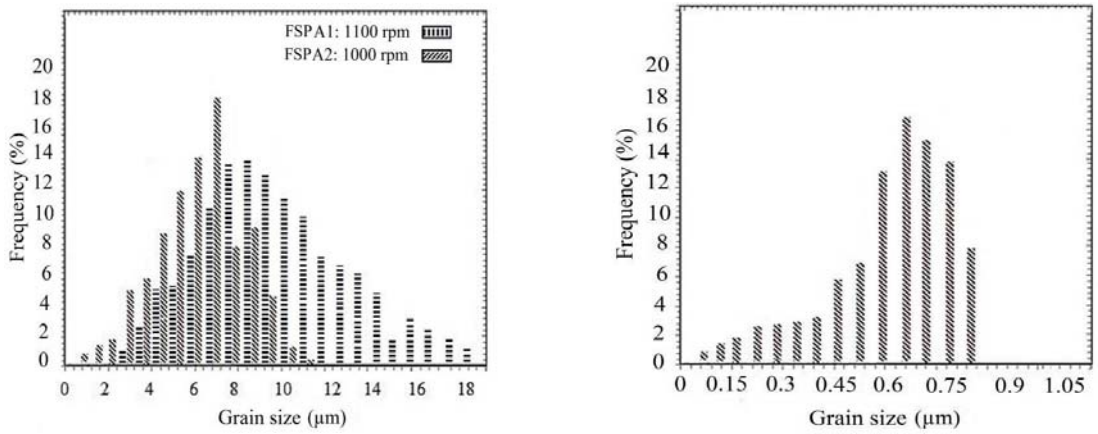

Fig. 5. Grain size distribution histograms of the samples of a) A2 & A1 and b) N2

within 1 to 11 µm with an average grain size of 7.2 µm. The formation of smaller grains in the SZ of A2 joint is as a result of the fact that faster cooling rate during the welding inhibits the growth of the recrystallized grains that will lead to the formation of smaller recrystallized grain structure. The average grain sizes in the SZ of the RT FSPed weldments are in accordance with average grain size values (in the range of 6- 10 µm) reported in the literature cited in this study. The size distribution investigations can also give information on the grain growth mechanism of the recrystallized grains. It is known that the grains with high stored energy can grow by two mechanisms, namely normal and abnormal grain growth or secondary recrystallization. The narrower distribution of grain sizes shows that the kinetic of the grain growth in the A2 followed Hillert's distribution as the maximum radius is about 1.8 times larger than the average radius value. Therefore, more uniform and normal growth occurred in the SZ of A2 compared to A1 and size distribution follows an asymptotic law characteristic [43].

The average grain size in the SZ of the RC FSPed joint is significantly smaller than that of RT FSPed joints. The mean grain size in the SZ of N2 joints is approximately 0.6±0.2 µm with low fractions of nano-sized grains (45- 100nm), as can be seen in Fig 5. Moreover, more than 60% of the grains are in the range of 600- 700 nm. The formation of UFG structure is the sign of the transformation of LAGBs to high angle ones as a result of intensive plasticization of the metal during the processing by the FSP tool. In addition, very high amount of stored energy and great amount of dislocations (see below) should have been contributed to the dynamic recrystallization process. The mentioned factors are highly beneficial in promoting nucleation and small grains in the SZ of the FSPed joints. It is found that sinking the introduced heat from both upper and lower surfaces during the FSP

Table 2. The measured dislocation densities, sub-grain sizes and grain size of the different processed zones for the BM, N2 and A2 joints

Zone	Rapid cooling – 1400 rpm (FSPN2)			Air cooling – 1000 rpm (FSWA2)		
	Dislocation density (10^{14} m^{-2})	Sub-grain size (nm)	Grain size (μm)	Dislocation density (10^{14} m^{-2})	Sub-grain size (nm)	Grain size (μm)
BM	2.3± 0.20	140	75	2.3± 0.20	140	75
HAZ	5± 0.50	100	5	1.7± 0.15	125	12
TMAZ	6.5± 2.3	35	3.2	2.1± 3.20	100	11.7
SZ	3.5± 0.15	8.5	0.67	1.5± 0.35	84	8.5

led to relatively identical microstructural characteristics of the grains in the center and bottom regions of the SZ. However, an assessment of TEM micrographs presented in some papers cited in this study shows that the density of dislocations in the weld area of in-air FSWed joints is not considerable. Further quantitative results (below) also agree well with the later statement.

The characteristics of the grain boundaries were investigated by plotting the misorientation angle distribution (MAD) profiles obtained from EBSD analyses. Disorientation angles can be used to estimate the stored energy introduced to the metal from a working process. The stored energy is often considered to be a driving force for primary recrystallization process and can be calculated by Read-Schockley relationship [44, 45]. Thus, the MAD profiles *per se,* can lead to qualitative results related to the stored energy of the cooled and non-cooled joints in their present state as well as in some post-heat treatments of the joints. The MAD histograms show that the BM consists of 94% HAGBs, as can be seen in Fig 6. There is a noticeable difference between the microstructure and grain boundary character related to the SZ and its surrounding area. Most fractions of LAGBs in all the samples are related to TMAZ. In other words, as expected, most fractions of dislocations and/or sub-grain boundaries are formed in the TMAZ of the joints. Microstructural evolution in TMAZ of Al-Mg-Si series aluminum alloys is a well-studied issue and has been described in previous investigations [46-49]. In this study, the width of TMAZ was measured to be no more than 0.7 mm for the RT FSPed joints and no more than 0.3 mm for RC FSPed joints. Generally, the TMAZ has the finest width among all the zones in the processed area and its microstructure consists of heavily deformed grains. However, the extent of deformation depends on factors such heat input and severity of plasticization. Accordingly, dynamic recrystallization process takes place with a progressive transformation of stored dislocations to sub-boundaries and then to new recrystallized grains [48, 49].

The fraction of LAGBs in the TMAZ of N2 joint is about 49%, which is a significant fraction of LAGBs when compared with the corresponding value of the BM and other joints. It should be pointed out that this joint had the fastest cooling rate and the most intensive localized plastic flow during the processing compared with the other samples. The high amount of LAGBs, even after the processing, confirms the presence of very high stored energy in the microstructure of the N2 sample. In the case of A1 and A2 samples, the TMAZ of A1 contains less LAGBs and more HAGBs compared to A2 joint. An incomplete dynamic recrystallization process is the only reason that can be responsible for the differences in the nature of the grain boundaries angles. The high fraction of LAGBs in the TMAZ of N2 and, to some extent, A2 joints compared with that of A1 can be attributed to the occurrence of partial dynamic recovery in these two cases. According to this assumption and considering the obtained data, the partial recovery and recrystallization processes during the processing were much more pronounced in N2 joint. The quantitative microstructural evaluations obtained from high resolution XRD experiments are presented in Table 2. The data are in accordance with the MAD histograms, presented in Fig 6.

Thus, the dislocation density in the SZ of N2 joint ($3.5\times10^{14}m^{-2}$ in SZ) is substantially higher

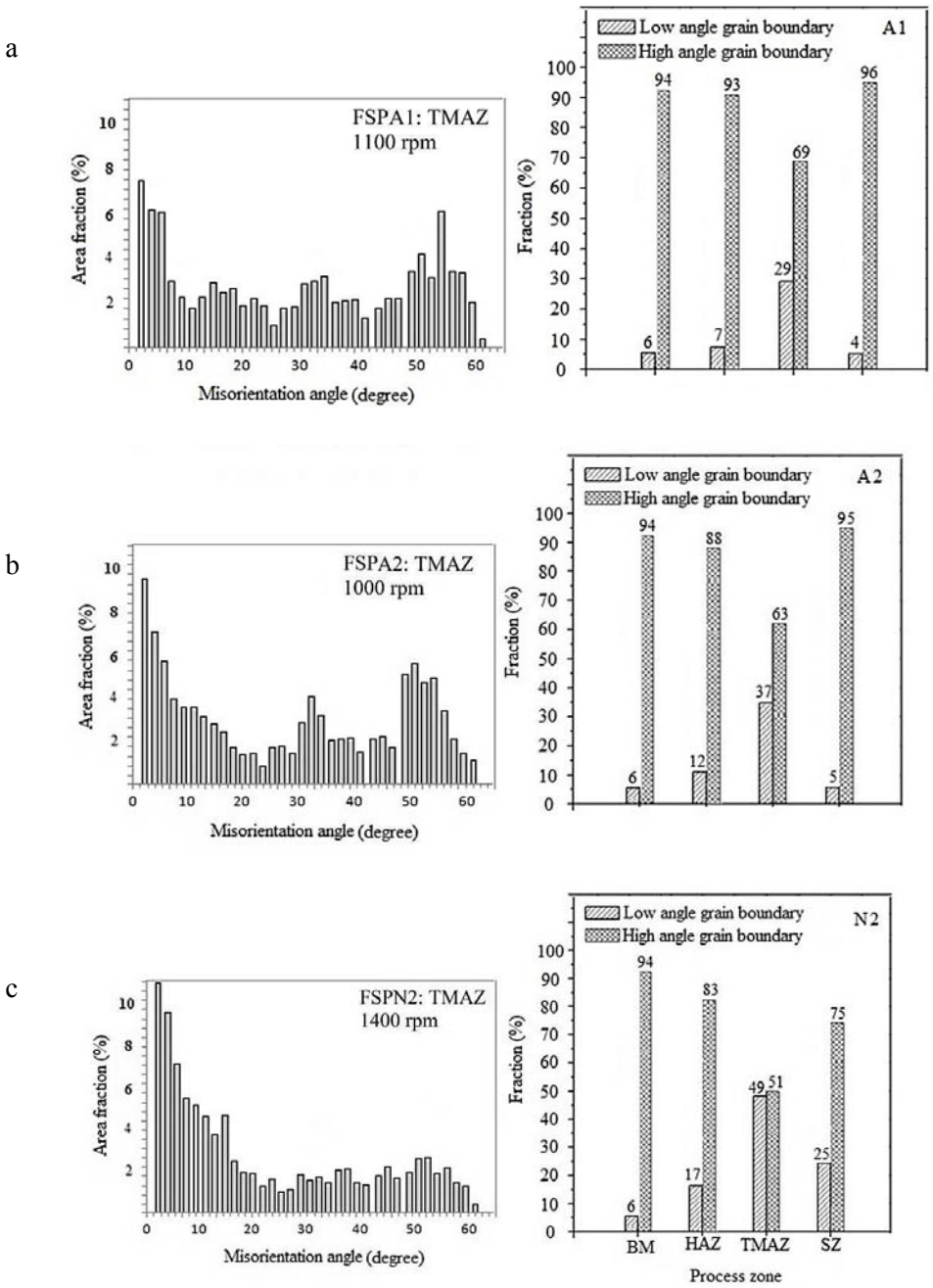

Fig. 6. Disorientation angle distribution histograms and fraction of HAGBs and LAGBs related to different zones of the FSPed joints a) A2, b) A1 and b) N2

compared with that of A2 joint ($1.5\times10^{14}m^{-2}$). This value is also higher than that of the BM ($2.3\times10^{14}m^{-2}$). The sub-grain size of the HAZ and TMAZ of the RT FSPed joints did not change significantly with respect to the BM. The small changes in the size of sub-grains in the HAZ towards the TMAZ are similar to the data reported by Woo et al. [32]. However, in the case of the RC FSPed joint, i.e. N2, there is a considerable difference in the sub-grain size when moving from the BM to the TMAZ, decreasing from 140 nm to 35 nm. The TMAZ of the N2 joint with the finest sub-grain structure showed the highest dislocation density with a value of 6.5×10^{14} m^{-2} among all the regions related to all the joints. The extremely high value of dislocation density in the TMAZ of the cooled FSPed joint has not been reported

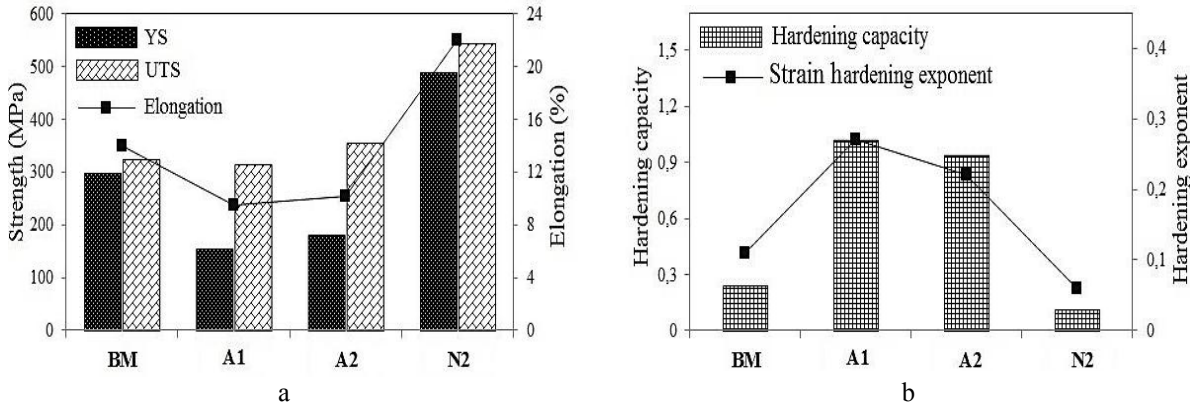

Fig. 7. (a) Tensile properties of the BM and FSPed AA 6061-T6 joints (YS: yield strength, UTS: ultimate strength, and El: elongation), (b) hardening capacity and strain hardening exponents

previously in any other processed aluminum alloys. The latter statement indicates the significant role of the liquid N_2 and the copper backing plate that functioned as strong cooling media and heat sink, respectively, in inhibiting the dynamic microstructural evolution of the alloy during a thermo-mechanical process.

The local strength of the joints is examined by room-temperature tensile experiment. So far, only limited investigations have been reported [24, 51] on the strain hardening of the FSWed weldments and, to our knowledge, no study has been carried out on the strain hardening of the UFG FSPed aluminum alloys with very high dislocation density. The work hardening behavior associated with dislocation movements during tensile deformation is evaluated by determining the ultimate and yield strengths of the joints, the results of which are plotted in Fig 7. The yield and ultimate strengths are 155±5 and 314±8 MPa for A1, 182±4 and 355±3 MPa for A2 and 488±5, 545±10 MPa for N2, respectively (The corresponding values for the BM are 299 MPa and 325 MPa). When discussing UFG structure and the plastic deformation behavior, strain hardening behavior should be taken into account as one of the crucial considerations in deformation behavior of the joints. Thus, the hardening capacities (H_c) of the processed samples are calculated according to the equation *(UTS/YS)* - 1, where *UTS* is the ultimate strength and *YS* is the yield strength. Also, stain hardening exponents are obtained by the equation: $\sigma = K\varepsilon^n$, where n is the strain hardening exponent, σ is the true stress, K is the strength coefficient and ε is the true strain [24, 50-53].

In the case of RT FSPed joints, the YS and UTS strengths are relatively close and noticeably lower than those of the BM and RC FSPN2. In contrast, the RT FSPed samples showed a twofold increase in the quantitative hardening values, i.e. H_c and n. The A1 joint showed the highest H_c with a value of 1.02 and the lowest value (0.11) was related to N2 joint. The H_c and n values of are slightly higher than the A2 sample that is a result of higher difference in YS and UTS. It should be noted that A1 experienced higher heat input and, consequently, bigger average grain size was present in the SZ of the sample. The results indicate that there are correlations between work hardening behavior and some metallurgical aspects that are directly related to the yield strength of the joints such as dislocation density and grain size. The strain hardening behavior of FSWed weldments has been the subject of some cited studies [24, 51], where it is argued that the high H_c and n in the FSWed samples is related to low dislocation density as a result of a complete recrystallization during the processing. In the case of N2, an interesting enhanced combination of strength and ductility is observed, as it is expected for UFG metals [1-3]. However, the results proposed that N2 shows a poorer strain hardening behavior when compared with the BM and RT FSPed joints due to its microstructural characteristics discussed above.

These strengthening parameters are strongly affected by the rate of plastic deformation and

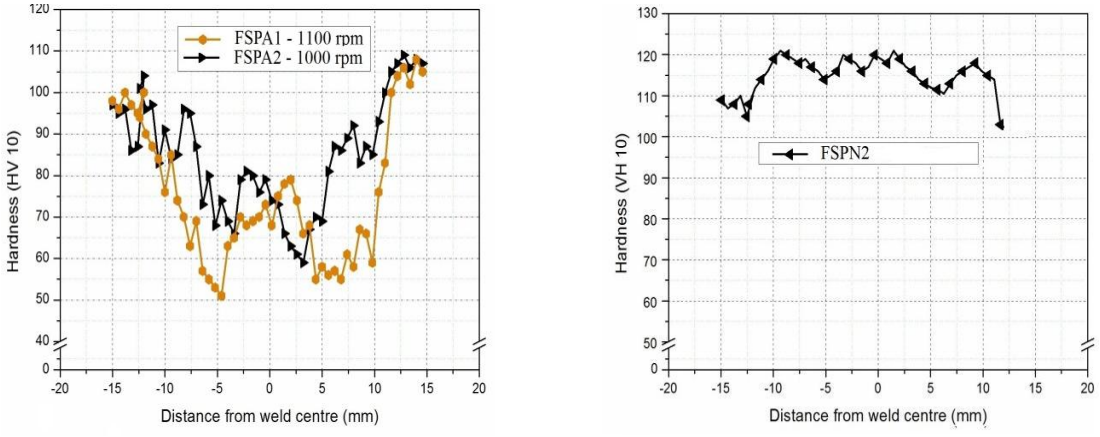

a b

Fig. 8. Microhardness profiles of the FSPed samples, a) A2 & A1 and b) N2

thermal history of the samples. As a result of the significantly larger number of dislocations in the BM and N2, the resistance to the dislocation movement increased and higher applied stresses (YS) were needed to deform the tensile specimens. Also, as a matter of fact, the YS is strongly influenced by the grain size based on the Hall-Petch relationship [16]. Thus it was expected for the FSPed joint to have significantly higher YS compared with the other joins. In contrast, RT FSPed joint required lower stress to start plastic deformation as a result of its recrystallized and annealed-like microstructure with much less densities of dislocations.

The very high strength of the N2 indicates that in addition to the pronounced role of the evolved precipitates, the other microstructure changes such as dislocation strengthening are crucial hardening contributions to the critical resolved shear stress (CRSS) of the grains. But it should be considered that all microstructural parameters such as grain and sub-grain size, second phase particles and dislocation density contribute to the mechanical properties of precipitate strengthened aluminum alloys [54]. Hence, in addition to the above discussion, the role of precipitates in the tensile properties of the joints should also be considered. Although characterization of the evolved second phase particles is not in the scope of this study, it should be mentioned that there is a difference in precipitate character, size and distribution in the SZ and TMAZ due to different thermal gradients and different degree of material flow. Thus, normally less strength in SZ of the RT FSPed joints is expected compared with the BM due to the changes in the characteristics of strengthening precipitates. The softening takes place due to the dissolution of strengthening second phase particles and grain coarsening that were caused by relatively high temperatures introduced into the SZ during the FSP (see Fig 3).

Microhardness profiles of the specimens that were obtained along the mid-thickness of the transverse cross section are shown in Fig 8. The first impression out of the hardness results is that the hardest zone is related to the SZ of N2 and the values are in range of 110-120 HV, which is even harder than the BM with an average hardness value of 105±5 HV. There is also a large difference between the hardness values for N2 joint compared with those of the A1 and A2 joints. The hardness of the SZ related to these samples decreased considerably from the hardness values of the BM by about 55-60%. The differences in the hardness values can be divided into two distinct discussions; the difference between RC FSPed joint and the RT FSPed joints and the differences in different regions of the RT FSPed joints. When discussing about the difference between the hardness values of the cooled and non-cooled joints, the thermal history (including the peak temperatures and the cooling rates) of the samples must be taken into account. Because it should be kept in mind that the studied alloy is a heat treatable Al alloy and the main changes in the hardness values are normally considered

to be due to the changes in the state of precipitation. Based on a fairly old work done by Sato et al. [55] the most important strengthening precipitate, i.e. β´´-Mg_5Si_6, in an Al-Mg-Si FSWed joints is not stable at temperatures higher than 353°C. It is also reported that the β´´phase starts to grow when the peak temperature reaches to 302°C. According to the thermal profiles shown in Fig 3, the temperature varied between 305 to 180°C in the N2 joint, while a peak temperature of about 470°C was measured in the RT FSPed joints during the processing. As it was discussed before, the peak temperatures of A1 and A2 joints were high enough to entail a solution heat treatment in the processed zones. However, the N2 joint experienced much lower temperature compared with the RT FSPed joints. It should also be considered that the cooling rate of the N2 joint was about 3 times faster than that of the A1 and A2 joints. There are some other metallurgical differences such as much higher density of dislocations (by a factor of 3) and much smaller grain size (by a factor of 10-13) in the SZ of the N2 joint compared to the A1 and A2 joints. Regarding the precipitation state of the joints, as the peak temperature in the weld area of the N2 joint was well below the solvus temperature and just slightly more than the growth temperature the β´´ phase, it is suggested that the needle-shape precipitates may not dissolve or grow significantly during the processing as a result of its low peak temperature and fast cooling rate obtained by the backing plate and the coolant. The latter suggestion is in accordance with the hardness profiles, where the hardness values of the processed regions of the N2 joint did not decrease, but increased instead, when compared with the hardness of the BM. However, any strong judgment regarding the state of the precipitations, the exact effect of the reduced grain size and high density of dislocations on the mechanical behavior of the N2 joint needs more dedicated studies. It is worth mentioning that the task of characterization of the precipitates that are evolved in different processed areas of the cooled FSPed joints that led to such different mechanical properties is the subject of our ongoing research.

From the thermal history and the hardness profiles, one can also conclude that the A1 and A2 joints are not any more in the T6 condition. The differences observed in different regions of the A1 and A2 joints are the result of softening and recrystallization of the microstructure in the SZ. Furthermore, the hardness profiles show that the center lines of A1 and A2 joints are slightly harder than their surrounding areas, i.e. AS and RS. This could also be explained with respect to the thermal history of the samples that is maximum in the center of the welds pointing the chances of later aging in the SZ of the RT FSPed joints [39, 56, 57]. As it was expected, the RT FSPed specimens failure took place either at the AS or RS during the tensile tests where the least microhardness values were measured.

4. Conclusions

In summary, FSP on AA 6061-T6 is performed and UFG structures with an average grain size of about 600 nm with predominant HAGBs of about 75% in the SZ were fabricated. A new experimental set-up with two powerful heat sink sources was used in this study. A rapid quenching was applied using a copper anvil with internal tunnels for circulating the coolant followed by spraying liquid N_2 to upper surface of the sheets during the processing to freeze the dynamic microstructural processes as much as possible. The sound FSPed joints indicated that this modified way of heat transferring can be considered a standardized FSP joining methodology. The occurrence of dynamic recovery and recrystallization and grain growth in the processed area of the joints were investigated. The higher heat input and on the other hand the faster cooling rate in the FSPed joints caused a partial dynamic recovery and recrystallization processes of the deformed microstructure. The quantitative analysis by high resolution XRD showed that the dislocation density in the SZ of the cooled FSPed joints was about 1.5 times higher than that of the BM. The most density of dislocations was measured in the TMAZ of the cooled sample with a value of about 6.5×10^{14} m^{-2}. The dislocation density in the TMAZ of the non-cooled joints was substantially lower by a factor of about 3. Considerably better YS,

UTS and microhardness values were achieved in the SZ of cooled joints compared with those of the BM. The values were significantly higher than those of the air-cooled FSP joints, while the strain hardening capacity and hardening exponent values were consistently smaller than those of the non-cooled FSPed joints. It is suggested that the latter behavior is attributed to the presence of undissolved precipitates as well as the significantly larger number of process induced dislocations and smaller grain sizes in the cooled FSPed joint.

Acknowledgment

The authors would like to thank Mr. Bahman Abbasizadeh (KIAU) for the helps with the NDT inspections and hardness measurements. Mr. Masoud Rashidi, Department of Materials and Microstructure, Chalmers University of Technology, is also deeply acknowledged for his comments and assistance with the XRD measurements.

References

1. H. Hasegawa, S. Komura, A. Utsunomiya, Z. Horita, M. Furukawa, M. Nemoto M, Mater. Sci. Eng. A. 265, 1999, pp. 188-196.
2. R. Z. Valiev, R. K. Islamgaliev, I.V. Alexandrov, Prog. Mater. Sci. 45, 2000, pp. 103-189.
3. M. Umemoto, T. Todaka, J.L. Tsuchiya, Mater. Sci. Forum. 503, 2006, p. 11-8.
4. C. M. Hu, C. M. Lai, P. W. Kao, N. J. Ho, J. C. Huang, Mater. Chara. 61, 2010, pp. 1043-1053.
5. N. Kumar, R.S. Mishra, Mater. Chara. 74, 2012, pp. 1-10.
6. K. T. Park, H. J. Kwon, W. J. Kim, Y. S. Kim, Mater. Sci. Eng. A. 316, 2001, pp. 145-152.
7. Y. J. Kwon, I. Shigematsu, N. Saito, Mater. Trans. 45, 2004, pp. 2304-2311.
8. D. Orlov, Y. Todaka, M. Umemoto, Y. Beygelzimer, Z. Horita, N. Tsuji, Mater. Sci. Forum 604, 2009, pp. 171-178.
9. H. Alihosseini, G. Faraji, A.F. Dizaji, K. Dehghani, Mater. Chara. 68, 2012, pp. 14-21.
10. R. S. Mishra, M. W. Mahoney, S. X. McFadden, N. A. Mara, A. K. Mukherjee, Scr. Mater. 42, 2000, pp. 163-168.
11. R. S. Mishra, M. W. Mahoney, Mater. Sci. Forum. 507, 2001, pp. 357-359.
12. Z. Y. Ma, R. S. Mishra, M. W. Mahoney, Acta Mater. 50, 2002, pp. 4419-4430.
13. A. H. Feng, Z. Y. Ma, Scr. Mater. 56, 2007, pp. 397-400.
14. Y. Morisada, H. Fujii, T. Nagaoka, M. Fukusumi, Mater. Sci. Eng. A. 419, 2006, pp. 344-348.
15. J.-Q Su, T. W. Nelson, C. J. Sterling, J. Mater. Res. 18, 2003, pp. 1757-1760.
16. C. G. Rhodes, M. W. Mahoney, W. H. Bingel, M. Calabrese, Scr. Mater. 48, 2003, pp. 1451-1455.
17. Z. Y. Ma, R. S. Mishra, M. W. Mahoney, R. Grimes, Mater. Sci. Eng. A. 351, 2003, pp. 148-153.
18. I. Charit, Z. Y. Ma, R. S. Mishra, In: Taleff EM, Friedman PA, Krajewski PE, Mishra RS, Scroth JG, editors. Warrendale (PA), TMS, 2004.
19. M. Esmaily, A. Shokuhfar, Def. Diff. Forum 297, 2010, pp. 1116-1121.
20. W. Woo, H. Choo, D. W. Brown, Z. Feng, Metal. Mater. Trans. A. 38A, 2007, pp. 69-76.
21. M. El-Rayesa, E. A. El-Danafa, J. Mater. Proc. Technol. 212, 2012, pp. 1157-1168.
22. K. Elangovan, V. Balasubramanian, Mater. Desig. 29, 2008, pp. 362-373.
23. W. Woo, H. Choo, D. W. Brown, Z. Feng, P. K. Liaw, Mater. Sci. Eng. A. 437, 2006, pp. 64–69.
24. W. Woo, Z. Feng, X.-L. Wang, D.W. Brown, B. Clausen, K. An, H. Choo, C.R. Hubbard, S.A. David, Sci. Technol. Weld. Join. 12, 2007, pp. 298–303.
25. C. I. Chang, X. H. Du, J. C. Huang, Scr. Mater. 57, 2007, pp. 209-212.
26. K. Poorhaydari, B. M. Patchett, D. J. Ivey, Weld. J. 48, 2005, pp. 149S-155S.
27. P. Suortti. The Rietveld Method, R.A. Young (Ed.). Oxford University Press, Oxford, IUCr Monographs on Crystallography. pp. 167-185.
28. M. A. Krivoglaz. Theory of X-ray and Thermal Neutron Scattering by real Crystals. Plenum Press, New York, pp. 1969:258.
29. T. Ungar, H. Mughrabi, D. Ronnpagel, M. Wilkens, Acta Metall. 32, 1984, pp. 333-342.
30. A. Sarkar, A. Bhowmik, S. Suwas, Mater. Sci. Proc. 94, 2009, pp. 943–948.

31. A. Sarkar, P. Mukherjee, P. Barat, Mater. Sci. Eng. A. 485, 2008, pp. 176–181.
32. W. Woo, T. Ungar, Z. Feng, E. Kenik, B. Clausen, Metall. Trans. A. 41, 2010, pp. 1210-1216.
33. M. W. Mahoney, R. S. Mishra, ASM International. 2007, p. 42.
34. G. G. Roy, R. Nandan, T. DebRoy, Sci. Tech. Weld. Join. 11, 2006, pp. 606-608.
35. M. Esmaily, S. N. Mortazavi, P. Todehfalah, M. Rashidi, Mater. Desig. 47, 2013, pp. 143-150.
36. K. Lu, M.L. Sui, Scr. Mater. 28, 1993, pp. 1465-1470.
37. W. Zhang, H. Wang, R.W. Scattergood, J. Narayan, C.C. Koch, Acta Mater. 50, 2002, pp. 3995-4004.
38. T. W. Nelson, J. Q. Su, R. Mishra, M. Mahoney, Acta Mater. 51, 2003, pp. 713-729.
39. G. Liu, L.E. Murr, C.S. Niou, J.C. McClure, F.R. Vega, Scr. Mater. 37, 1997, pp. 355-361.
40. S. Lim, S. Kim, C.G. Lee, S.J. Kim, Metall. Mater. Trans. A. 35, 2004, pp. 2829-2835.
41. S. R. Ren, Z. Y. Ma, L. Q. Chen, Scr. Mater. 56, 2007, pp. 69-72.
42. A. Scialpi, L. A. DeFilippis, P. Cavaliere, Mater. Desig. 28, 2007, pp. 1124-1129.
43. P. A. Manohar, D. P. Dunne, T. Chandra, C. R. Killmore, ISIJ Int., 36, 1996, pp. 194-196.
44. W. Read, W. Shockley, Phys. Rev. 78, 1950, pp. 275-289.
45. M. Taheri, H. Weiland, A. Rollett, Metall. Mater. Trans. A. 37, 2006, pp. 19-25.
46. M. Cabibbo, E. Meccia, E. Evangelista, Mater. Chem. Phys. 81, 2003, pp. 289-292.
47. R. W. Fonda, J. F. Bingert, Metall. Mater. Trans. A. 35, 2004, pp. 1487-1499.
48. S. H. Kang, W. H. Bang, J. Cho, H. Han, H.H. Oh, C.G. Lee, S.J. Kim, Mater. Sci. Forum 905, 2005, pp. 495-497.
49. C. Hamilton, S. Dymek, M. Blicharski, W. Brzegowy, Sci. Tech. Weld. Join. 12, 2007, pp. 702-707.
50. J. Luo, Z. Mei, W. Tian, Z. Wang, Mater. Sci. Eng. A. 441, 2006, pp. 282–290.
51. N. Afrin, D. L. Chen, X. Cao, M. Jahazi, Scr. Mater. 57, 2007, pp. 1004-1007.
52. G. E. Dieter, Mechanical Metallurgy, McGraw-Hill, New York, Third edition, 1986.
53. W. F. Hosford, Mechanical Behavior of Materials, Cambridge University Press, New York, 2005.
54. M. J. Starink, A. Deschamps, S. C. Wang, Scr. Mater. 58, 2008, pp. 377–382.
55. Y. S. Sato, H. Kokawa, M. Enomoto, S. Jogan, Metall. Trans. A. 30,1999, pp. 2427-37.
56. B. Heinz, B. Skrotzki, Metall. Mater. Trans. B. 33, 2002, pp. 489-498.
57. C. Gallais, A. Denquin, Y. Brechet, G. Lapasset, Mater. Sci. Eng. A. 496, 2008, pp. 77-89.